Design of Pd Graphene Au Nanorod Nanocomposite Catalyst for Boosting Suzuki Miyaura Coupling Reaction by Assistance of Surface Plasmon Resonance

doi: 10.1021/acs.jpcc.9b06609

Design of Pd-Graphene-Au Nanorod Nanocomposite Catalyst for Boosting Suzuki-Miyaura Coupling Reaction by the Assist of Surface Plasmon Resonance

Takeharu Yoshii,[†] *Yasutaka Kuwahara,*[†,‡] *Kohsuke Mori,*[†,‡] *and Hiromi Yamashita*[*,†,‡]

[†] Division of Materials and Manufacturing Science, Graduate School of Engineering, Osaka University, 2-1 Yamadaoka, Suita, Osaka 565-0871, Japan.

[‡] Elements Strategy Initiative for Catalysts & Batteries Kyoto University (ESICB), Kyoto University, Katsura, Kyoto 615-8520, Japan.

Corresponding Author

*E-mail: yamashita@mat.eng.osaka-u.ac.jp

Abstract

Visible-light boosting chemical reactions by surface plasmon resonance (SPR) have recently received much attention in photocatalysis. Although multiple types of plasmonic catalysts have been developed, the efficient utilization of SPR-induced hot-electrons remains to be a challenging task due to their ultrafast decay. In this study, structure-controlled Pd-graphene-Au nanorod nanocomposite catalysts are fabricated for maximizing hot-electron utilization in SPR-enhanced reactions. The characterization confirmed that highly-dispersed Pd clusters were deposited on a homogeneous reduced graphene oxide (rGO) layer-coated Au nanorods. The catalytic activity in the Suzuki-Miyaura coupling reaction was highly enhanced under visible-light irradiation due to the SPR of the Au nanorods, whose performance was superior to that without an rGO layer. Further experimental and calculation study demonstrated that the electro-conductive rGO layer plays a crucial role as an electron mediator for promoting hot-electron transportation from Au to Pd, which resulted in the reaction acceleration.

Introduction

Surface plasmon resonance (SPR) is a photon-induced collective oscillation of conduction electrons at the surface of a noble metal.[1,2] In particular, SPR in Au, Ag, and Cu nanoparticles (NPs) is strongly excited by light in the visible or near-infrared region, and therefore plasmonic nanostructures are attracting considerable interest in photocatalysis. [3-7] In plasmonic catalysts, energetic electrons produced by SPR, so-called hot-electrons, are transferred into anti-bonding orbitals of reaction substrates or intermediates, which can facilitate specific reactions or change product selectivity. [8-10] However, pure plasmonic metal NPs (Au, Ag, and Cu NPs) are relatively inactive as photocatalysts, because of ultrafast decay of the SPR-induced hot-electrons through electron-phonon scattering and the inherent catalytic inertness of these NPs. [11,12] The most popular approach to overcome this problem is a combination of plasmonic metal and semiconductor, in which the SPR-induced hot-electrons are transferred to the semiconductor and utilized for reaction promotion, but applicable reactions are limited. [13-15] As another strategy, a direct hybridization of plasmonic metal NPs and catalytically active metals, such as Pd, Pt, and Rh, has been recently studied. [16-19] These bimetallic nanostructures have been reported to accelerate a wide range of chemical reactions under visible-light irradiation. Unfortunately, the hot-electron utilization efficiency is still quite low, because visible-light absorption is diminished by the second metal and electron-phonon dissipation is likely to occur at the interfaces between the two metals, which eventually leads to a low catalytic performance. [19,20] Thus, a new plasmonic bimetallic nanostructure is needed to maximize hot-electron utilization efficiency. Graphene has an exceptionally high electron mobility, [21] and therefore it is conceivable that graphene can quickly transfer SPR-induced electrons to the catalytic active metals. Herein, we develop reduced graphene oxide (rGO)-coated Au nanorods (NRs) as a support for a Pd cluster catalyst. In the Suzuki-

Miyaura coupling reaction, SPR-driven large activity enhancement was shown under visible-light irradiation, and its performance was higher than that without an rGO layer. It was found that the rGO layer acted as an electron-mediator between active Pd sites and Au NRs; thus, the utilization efficiency of plasmon-induced hot-electrons was improved, enhancing the activity.

Methods

Materials

Sulfuric acid (H_2SO_4), sodium nitrate ($NaNO_3$), potassium permanganate ($KMnO_4$), hydrogen peroxide (H_2O_2), hydrochloric acid (HCl), hydrogen tetrachloroaurate(III) tetrahydrate ($HAuCl_4 \cdot H_2O$), sodium borohydride ($NaBH_4$), silver nitrate ($AgNO_3$), L(+)-ascorbic acid ($C_6H_8O_6$), disodium tetrachloropalladate(II) (Na_2PdCl_4), iodobenzene (C_6H_5I), phenyl boronic acid ($C_6H_7BO_2$), potassium carbonate (K_2CO_3), biphenyl ($C_{12}H_{10}$), ethyl acetate ($C_4H_8O_2$), and ethanol (C_2H_6O) were purchased from Nacalai Tesque Inc. Cetyltrimethylammonium bromide ($C_{19}H_{42}BrN$) and naphthalene ($C_{10}H_8$) were purchased from Wako Pure Chemical Ind. Co., Ltd. Fumed silica (SiO_2) (S_{BET} = 395 m^2/g) and potassium bromide ($KBrO_3$) were purchased from Sigma-Aldrich Co. LLC. Graphite powder and phenylboronic acid ($C_6H_7BO_2$) were obtained from Kishida Chemical Co., Ltd and Tokyo Chemical Industry Co., Ltd, respectively. All chemicals were used as received without further purification.

Synthesis of graphene oxide (GO)

Graphene oxide (GO) was synthesized by modified Hummer's method[22]. H_2SO_4 (115 mL) was slowly added to graphite powder (5.0 g). After cooling to 0°C in an ice bath, $NaNO_3$ (2.5 g) and $KMnO_4$ (15.0 g) were carefully added to the mixture under stirring, and then the temperature rose to 35°C. After 60 min of stirring, H_2O (225 mL) was slowly added to the suspension and stirred for 60 min. A mixture of 30% H_2O_2 (50 mL) and H_2O (700 mL) was added, and the suspension was washed by centrifugation (6000 rpm, 30 min) and filtered. The filtrate was added to HCl (5 M, 100 mL) and stirred for 60 min. The resultant suspension was centrifuged (6000 rpm, 60 min), filtered, and dried under vacuum for one day. The product was ball-milled (800 rpm, 10 min, 2 times) to obtain GO powder.

Synthesis of nanosized GO

Nanosized GO was prepared by a reported procedure with modification[23]. The prepared GO powder (200 mg) was dispersed in 500 mL of H_2O and ultrasonicated for 24 h for exfoliation of GO sheet. The suspension was centrifuged (6000 rpm, 15 min, 4 times) and the supernatant was collected. The resultant suspension was filtered by 5C filter paper to remove un-exfoliated large GO, and a light-brown colored nanosized GO suspension was obtained.

Synthesis of Au nanorods (NRs)

Au NRs were synthesized using a seed-mediated growth method[24,25]. The seed solution was prepared by adding a freshly prepared $NaBH_4$ solution (10 mM, 0.6 mL) to a mixture of $HAuCl_4$ (10 mM, 0.25 mL) and cetyltrimethylammonium bromide (CTAB) solution (100 mM, 9.75 mL)

under vigorous stirring. The obtained brown solution was kept at room temperature for 1 h. In order to prepare the growth solution, $HAuCl_4$ (10 mM, 10 mL) and $AgNO_3$ (10 mM, 2 mL) were added to a CTAB solution (100 mM, 200 mL). Subsequently, a freshly prepared ascorbic acid solution (100 mM, 1.6 mL) and HCl (1.0 M, 4 mL) were added, and the orange color of the solution changed to clear due to the reduction of Au^{3+} to Au^{1+}. Finally, the prepared seed solution (50 μL) was injected under gentle stirring and the mixture was left undisturbed at room temperature overnight, and a red-colored AuNR colloid was obtained. No sedimentation was observed in the colloidal solution even after 1 month.

Synthesis of Pd/Au@rGO/SiO_2

The rGO coated Au NR supported Pd catalyst (Pd/Au@rGO/SiO_2) was prepared by a bottom-up synthetic method. The AuNR colloids (20 mL) were centrifuged at 6000 rpm for 15 min to remove the excess of surfactant and the precipitants were re-dispersed in 20 ml of H_2O. The nanosized GO suspension (10 mL) was added to an Au NR colloid suspension (20 mL) and left at room temperature for at least 6 h. The obtained colloids were denoted as Au@rGO-10. Na_2PdCl_4 solution (10 mM, 56.4 μL) was added to Au@rGO-10 and stirred for 30 min (denoted as Pd/Au@rGO-10). Subsequently, 20 mg of fumed silica was added to the suspension. After 60 min of stirring, the solvent water was removed at 70°C under vacuum with a rotary evaporator. The prepared powder was reduced by hydrogen at 50°C for 30 min to yield Pd/Au@rGO-10/SiO_2. The amount of Au and Pd in Pd/Au@rGO-10/SiO_2 was determined to be 4.33 and 0.17 wt%, respectively, from ICP analysis. Furthermore, the amount of nanosized GO suspension was changed to 5, 20, and 40 mL in the synthetic procedure of Pd/Au@rGO-10/SiO_2, and catalysts

with various rGO amounts were obtained. The catalysts were denoted as Pd/Au@rGO-x/SiO_2 (x: 5, 20, 40).

Synthesis of reference catalysts

Reference catalysts were synthesized by a similar procedure as Pd/Au@rGO/SiO_2. Au@rGO/SiO_2 was prepared by the impregnation of Au@rGO-10 on fumed silica instead of Pd/Au@rGO-10. Pd/GO was synthesized by the impregnation of Na_2PdCl_4 solution (10 mM, 56.4 μL) on GO (20 mg) and hydrogen reduction as mentioned above (50°C, 30 min). The content of Pd in Pd/GO was determined by ICP analysis as 0.21 wt%. Pd/Au/SiO_2 was prepared without the addition of the nanosized GO suspension in the Pd/Au@rGO-10/SiO_2 synthesis. The amount of Au and Pd in Pd/Au/SiO_2 was determined to be 3.31 and 0.14 wt%, respectively, from ICP analysis.

Characterization

Transmission electron microscopy (TEM) images were obtained using a field emission-transmission electron microscope (FE-TEM; Hitachi Hf-2000) operated at 200 kV. Scanning transmission electron microscopy (STEM) images and elemental mappings were obtained using a JEOL-ARM 200F equipped with a Kvex energy-dispersive X-ray detector (JED-2300T) operated at 200 kV. Powder X-ray diffraction (XRD) patterns were recorded using a Rigaku Ultima IV diffractometer with Cu Kα radiation (λ = 1.54056 Å). Thermogravimetric differential thermal analysis (TG-DTA) was carried out using a Rigaku thermogravimetry unit, Rigaku Thermo Plus EVO II series high temperature differential thermal balance TG-DTA, with temperature increasing

at a rate of 2°C/min up to 800°C. Raman spectroscopy measurement was performed using a laser Raman confocal microscope (Nanophoton, RAMAN-11) using an excitation wavelength of 532 nm through a 20x objective. UV visible absorption spectra were examined using a Shimadzu UV-2600 UV-vis spectrophotometer with a quartz cell (light-path length = 1.0 cm) at room temperature. The ultraviolet visible diffuse reflectance (UV-vis) spectra of the powdered samples were recorded using a Shimadzu UV-2450 spectrophotometer. Using $BaSO_4$ as a reference, absorption spectra were calculated using the Kubelka-Munk function. Inductively coupled plasma atomic emission spectroscopy (ICP-ES) was measured using a Nippon Jarrell-Ash ICAP-575 Mark II instrument.

Catalytic test

The catalytic performance was evaluated in the Suzuki-Miyaura coupling reaction[16]. In a typical procedure, the suspension containing ethanol (5.5 mL), phenylboronic acid (18.3 mg, 0.15 mmol), K_2CO_3 (20.8mg, 0.15 mmol), naphthalene (19.2 mg, 0.1 mmol) as an internal standard and the catalyst (10 mg) were added into a Pyrex glass reactor. The reactor was then sealed with a rubber septum, and the suspension was bubbled with Ar gas for 15 min. The reaction was initiated by the injection of iodobenzene (0.115 μL, 0.10 mmol) into the reactor using a syringe under continuous stirring at room temperature in the dark or under visible-light irradiation (500 W Xe lamp (SAN-EI ELECTRIC Co., Ltd. XEF-501S) with 420 nm long-pass filter). In order to prevent a temperature rise due to light irradiation, an external fan was equipped in the reaction system to maintain the temperature of the reactor. Products were examined by gas chromatograph (Shimadzu, GC-2014) using a frame ionization detector (FID) with a non-polar capillary column (TC-1, 60 m×0.32mm×0.25 μm) and gas chromatography-mass spectrophotometry (Shimadzu, GCMS-

QP2010 plus). A reaction with an electron scavenger was conducted using H_2O (5.5 mL) as a reaction solvent instead of ethanol in the typical procedure, and a $KBrO_3$ electron scavenger (83.5 mg, 0.5 mmol) was added in the reaction suspension just before the reaction initiation. The product was extracted with 2.0 mL of ethyl acetate and examined by the same method as mentioned above.

DFT calculation

All density functional theory (DFT) calculations were performed using the DMol^3 program in Materials Studio 17.2.[26,27] The generalized gradient approximation (GGA) exchange-correlation functional proposed by Perdew, Burke, and Ernzerhof (PBE) was combined with the double numerical basis set plus polarization functions (DNP). (i) A (5×2) graphene surpercell on a (3×3) Au (110) surface cell and (ii) a (7×2) graphene surpercell on a (6×3) Au (100) surface cell were employed for Au(110)/graphene and Au(100)/graphene models, respectively. The bottom 4 Au layers were fixed at the corresponding bulk position, and the top Au layer and the graphene layer were allowed to relax during geometry optimizations. A vacuum spacing was set to 30 Å to avoid nonphysical electronic interaction.

Results and discussion

The catalyst was prepared by a bottom-up two-step method (Scheme 1). In the first step, rGO-coated Au nanorods (Au@rGO) were synthesized using graphene oxide (GO) and Au NRs as precursors.[23] Au NR colloids were prepared by a typical seed-mediated growth method, [24,25] and

colloidal monodispersed Au NRs (25 nm diameter, 75 nm length, aspect ratio = 3) were observed using transmission electron microscopy (TEM) (Fig. 1Aa). GO was synthesized by a modified Hummer's method,[22] and the size of the GO was reduced through sonication and filtration. Subsequently, Au NR colloids (20 mL) and a designated amount of nanosized GO suspension were mixed to yield Au@rGO using the interaction between the positively-charged cetyltrimethylammonium bromide (CTAB) layer on the Au NR surface and the negatively-charged nanosized GO.[23,28] The introduced amount of nanosized GO suspension was changed from 5 to 40 mL, and each sample was denoted as Au@rGO-x (x: 5, 10, 20, 40). In the TEM image of Au@rGO-10 (Fig. 1Ab), the Au NR is completely surrounded by an rGO layer with a mean thickness of 2.8 nm. Moreover, in thermogravimetric differential thermal analysis (TG-DTA) under air flow (Fig. S1), Au@rGO-10 shows a 7% higher weight loss than Au NRs around 350°C, which corresponds to combustion of the rGO layer. These results demonstrate the successful coating of nanosized GO on an Au NR surface.

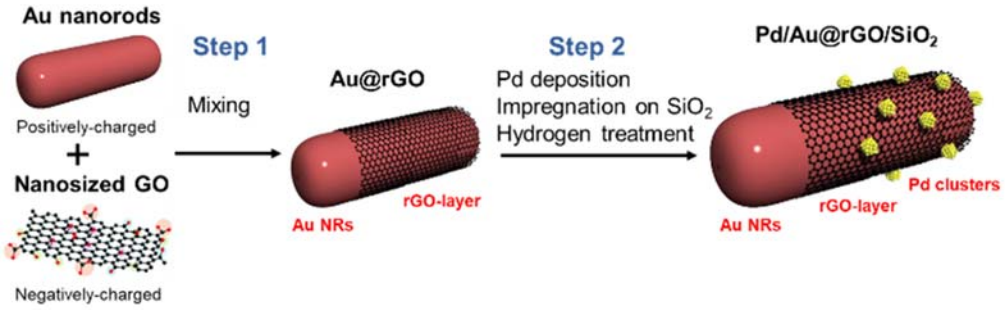

Scheme 1. Synthetic procedure for Pd/Au@rGO/SiO_2.

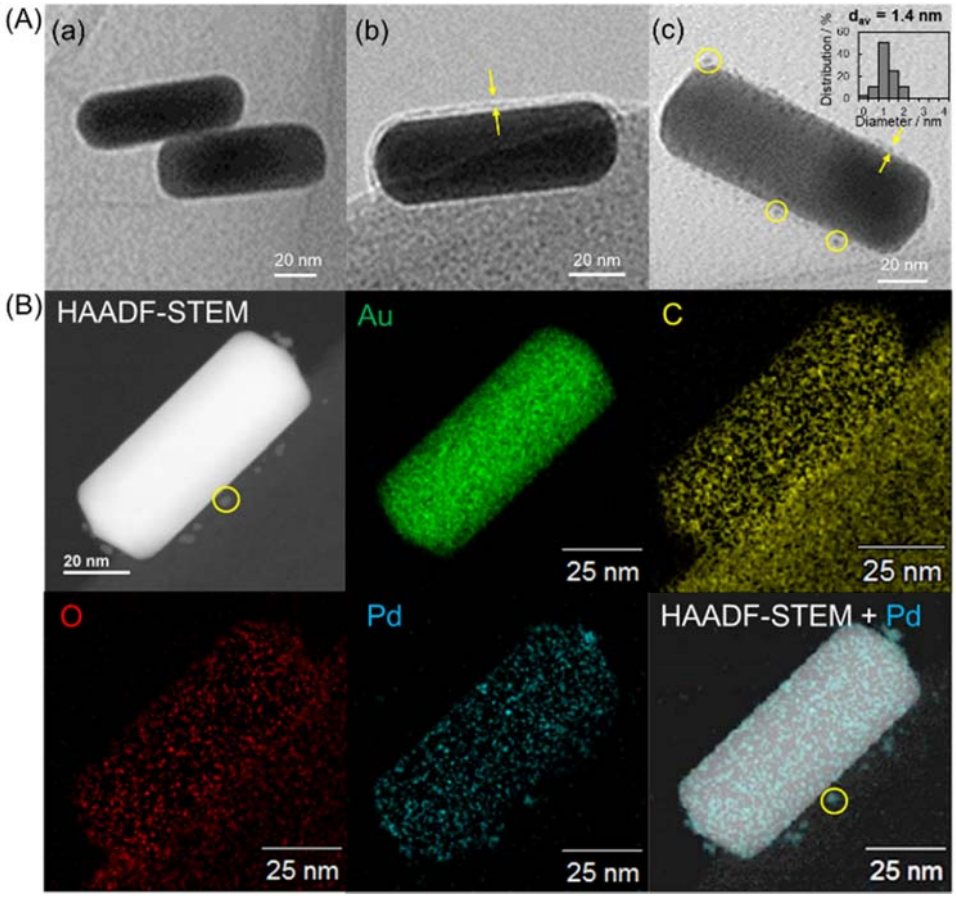

Figure 1. (A) TEM images of (a) Au NRs, (b) Au@rGO-10, and (c) Pd/Au@rGO-10. Inset in (c) shows a distribution diagram of the deposited Pd clusters. (B) HAADF-STEM image and the corresponding EDX mapping images of Pd/Au@rGO-10. Note: C and O signals shown in the lower-right part of the figure originated from the carbon grid used for the STEM measurement.

In the next synthetic step, Pd clusters were deposited onto the rGO layer of Au@rGO-x using Na_2PdCl_4 as a precursor. The obtained colloids (Pd/Au@rGO-x) were impregnated on fumed silica and treated with hydrogen at 50°C, and rGO-coated Au NR supported Pd catalysts (Pd/Au@rGO-x/SiO_2) were synthesized. Figure 1Ac shows TEM images of Pd/Au@rGO-10. Pd

clusters (circled in Fig. 1Ac) with a mean diameter of 1.4 nm are formed on the rGO layer. Figure S2 presents TEM images of Pd/Au@rGO-10 with a wider range, revealing the homogeneous coting of the rGO layer and high-dispersion of the Pd clusters. The structure is more clearly visualized by scanning transmission electron microscopy (STEM) and EDX elemental mapping images (Fig. 1B). In the high-angle annular dark-field (HAADF) STEM image of Pd/Au@rGO-10, a number of clusters are clearly located 2-3 nm away from the Au NR, indicating the existence of an rGO layer between the Au NR and the clusters. This is also supported by the observation of C and O signals in the vicinity of the Au NR. From Pd EDX mapping and the EDX spectra (Fig. S3), the clusters, shown in the HAADF-STEM image, were definitely composed of Pd species. These STEM-EDX results explicitly reveal that the rGO layer acts as a separator between Pd active sites and the Au NRs in the catalyst. In addition, the high degree of dispersion of Pd clusters is supported by the powder X-ray diffraction (XRD) patterns for Pd/Au@rGO-10/SiO_2, which have trace peaks that can be assigned to the Pd or PdO crystal structures (typically at 40.0° and 33.8°, respectively) (Fig. S4).

In the UV-vis absorption spectra (Fig. 2A), the nanosized GO suspension displays a typical UV adsorption band at 234 nm attributed to $\pi \rightarrow \pi^*$ transitions of C-C bonds and a shoulder peak around 300 nm due to $n \rightarrow \pi^*$ transitions of C=O bonds, [29,30] but it is almost transparent in the visible-light region. Colloidal Au NRs show two characteristic visible-light absorption bands at 520 nm and 720 nm, which are assigned to transverse and longitudinal surface plasmon resonance (TSPR and LSPR), respectively. [31] These visible-light absorption bands corresponding to the SPR of Au NRs are also observed in Au@rGO-10, and nearly the same absorption intensity is maintained even after rGO coating. In the UV region, the absorption intensity of Au@rGO-10 increases compared to Au NRs, owing to the rGO layer on the Au NRs. Moreover, the visible-

light absorption bands corresponding to the TSPR at 520 nm and LSPR at 720 nm of Au NRs are also exhibited by Pd/Au@rGO-10/SiO_2 in the visible diffuse reflectance spectrum (Fig. 2B). Thus, the rGO layer transmits visible-light to the surface of the Au NRs, and does not prevent the SPR of Au NRs.

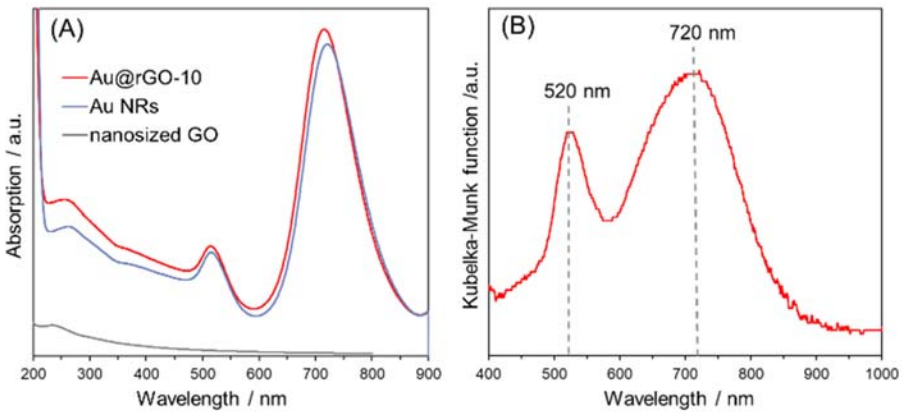

Figure 2. (A) UV-vis spectra of Au@rGO-10, Au NRs, and nanosized GO suspension. (B) Diffuse reflectance UV-vis spectrum of Pd/Au@rGO-10/SiO_2.

In the Raman spectra (Fig. S5), as-prepared GO shows the peaks at 1355 cm^{-1} and 1593 cm^{-1}, which can be attributed to D band and G band, respectively,[29] and the intensity ratio (I_D/I_G) is calculated to be 0.90. I_D/I_G of the nanosized GO increases to 0.97, suggesting partial reduction of the GO structure through sonication during the synthesis.[30] The prepared catalyst (Pd/Au@rGO-10/SiO_2) also exhibits peaks at the same Raman shifts, and more importantly, I_D/I_G increases to 1.02 during the catalyst preparation process, indicating that the coated nanosized GO was further reduced to an electro-conductive rGO state.[30,32]

The catalytic performance of the samples was assessed in the Suzuki-Miyaura coupling reaction between iodobenzene and phenylboronic acid under visible-light irradiation ($\lambda > 420$ nm, I = 380 mW · cm^{-2}) and in the dark at room temperature.[16] It was confirmed by gas chromatography-mass spectrophotometry that biphenyl (m/z = 154) was definitely produced in the catalytic reaction. As shown in Figure 3A, Pd/Au@rGO-10/SiO_2 exhibited 3.8 times higher activity under visible-light irradiation than in the dark. Moreover, the conversion of iodobenzene was 56% at 30 min of reaction when using Pd/Au@rGO-10/SiO_2 under visible light irradiation. The catalyst without Pd clusters (Au@rGO-10/SiO_2) gave no performance even under visible-light irradiation. The activity of the Pd catalyst without Au NRs (Pd/GO) in the dark was almost the same as that of Pd/Au@rGO-10/SiO_2, but no activity enhancement was observed under visible-light irradiation. Therefore, Pd species are the active sites in this catalytic system, and the large reaction promotion by Pd/Au@rGO-10/SiO_2 is driven by the SPR of Au NRs. Furthermore, a 2-fold activity enhancement of Pd/Au@rGO-10/SiO_2 was observed when using a 550 nm long-pass filter instead of the 420 nm filter (Fig. S6), which supports the fact that the LSPR of Au NRs facilitates the reaction (see Fig. 2B). In order to examine the effect of the rGO layer, a catalyst in which Pd species were directly deposited on Au NRs (Pd/Au/SiO_2) was prepared and tested. Pd/Au/SiO_2 showed an 11.0% yield in the dark, which is as high as Pd/Au@rGO-10/SiO_2 (12.0% yield). However, the activity of Pd/Au/SiO_2 under visible-light irradiation was only 1.5 times higher than in the dark, which suggests that the rGO layer in Pd/Au@rGO-10/SiO_2 provides a high performance in the SPR-enhanced reaction. A leaching test of Pd/Au@rGO-10/SiO_2 was performed using a hot filtration process after the reaction, and completely no activity was shown after the filtration. This reveals that the Pd species are not leached during the reaction and the reaction proceeds in heterogeneous mechanism. In addition, Figure S7 shows the XRD pattern of

Pd/Au@rGO-10/SiO_2 after the reaction. By comparing Figures S4 and S7, the peaks due to the Au crystal structure are maintained and the peaks assigned to the Pd or PdO remain at the trace level even after the reaction, suggesting that the high dispersion of Pd species is kept without aggregation.

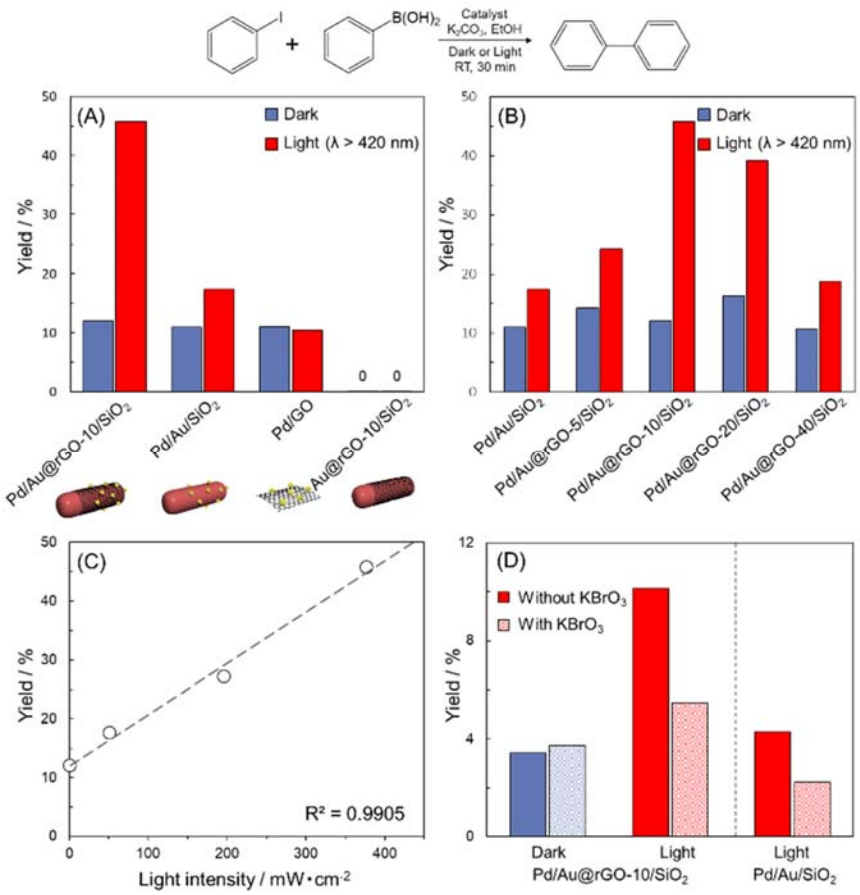

Figure 3. Comparison of catalytic activities in the Suzuki-Miyaura coupling reaction under visible-light irradiation (λ > 420 nm) or in the dark (A) over Pd/Au@rGO-10/SiO_2, Pd/Au/SiO_2, Pd/GO, and Au@rGO-10/SiO_2, and (B) over Pd/Au/SiO_2 and Pd/Au@rGO-x/SiO_2 (x: 5, 10, 20,

40). (C) Visible-light-intensity-dependent catalytic activity over Pd/Au@rGO-10/SiO_2. (D) Comparison of catalytic activities in the presence of an electron scavenger ($KBrO_3$).

In order to clarify the role of the rGO layer, catalysts with various rGO amounts were synthesized and tested in the reaction. In the TEM image of Pd/Au (Fig. S8a), it was confirmed that there is no rGO layer on the Au NRs, but Pd species cannot be distinguished from the surface of Au NRs. In the TEM image of Pd/Au@rGO-5 (Fig. S8b, c), which was synthesized with half the amount of nanosized GO but otherwise following the typical procedure, Au NRs are incompletely covered by rGO sheets with Pd clusters. When using double the amount of nanosized GO in the typical procedure (Pd/Au@rGO-20), the rGO layer surrounds the Au NR, but its thickness is inhomogeneous (Fig. S8d, e). Furthermore, aggregates composed of Au NRs and rGO sheets are formed when a 4-fold amount of nanosized GO was added (Fig. S8f), and these aggregates can be seen as precipitates in the colloidal suspension with the naked eye. In the UV-vis absorption spectra of a series of Pd/Au@rGO (Fig. S9), the UV absorption is enhanced corresponding to the amount of rGO added, but the visible-light absorption bands due to the SPR of Au NRs remain almost unchanged. Pd/Au@rGO-40 presents a lower absorption, because of the precipitants in the colloidal solution. When a series of Pd/Au@rGO was tested in the reaction (Fig. 3B), similar activities (11-16% yield) were observed in dark conditions, but Pd/Au@rGO-10/SiO_2 specifically provided a four-fold increase in reaction activity under light irradiation. The activity enhancement of Pd/Au@rGO-5/SiO_2 and Pd/Au@rGO-20/SiO_2 was limited to 1.7 and 2.4 times, respectively, probably due to the incomplete and irregular coverage of the rGO layer. The Pd/Au@rGO-40/SiO_2, which contained aggregates of Au NRs on an excess of rGO sheets, gave a

low yield. Considering these results, uniform coating of an rGO layer with an appropriate thickness is a key for highly-efficient reaction acceleration.

In order to elucidate the origin of the enhanced activity under light irradiation, the contribution of the photothermal effect was examined. The temperature increase of the reaction solution was only 3.0°C after 30 min reaction under visible-light, probably due to the low light-intensity ($\lambda > 420$ nm, $I = 380$ mW・cm^{-2}). Moreover, a clear linear correlation between visible-light intensity and reaction yield was observed (Fig. 3C). Therefore, the photothermal effect is negligible in this catalytic reaction, and it is speculated that SPR-induced hot-electrons facilitate the catalytic reaction. [7,8,13] To verify this speculation, a reaction with a $KBrO_3$ electron scavenger was conducted (Fig. 3D). [33,34] In the dark, Pd/Au@rGO-10/SiO_2 provided around 3.5% yield after 15 min of reaction regardless of the presence or absence of $KBrO_3$. On the other hand, the reaction yield decreased significantly from 10.1% to 5.4% when $KBrO_3$ was added under visible-light irradiation. An activity decrease in the presence of $KBrO_3$ was also observed when using Pd/Au/SiO_2. These results clearly show that hot-electrons, produced by the SPR of Au NRs, facilitate the reaction, and the large activity enhancement in Pd/Au@rGO-10/SiO_2 can be attributed to the improved utilization efficiency of hot-electrons due to the presence of the rGO layer.

To better understand the behavior of electrons in the catalysts, density functional theory (DFT) calculation was carried out. Since Au NR is well known to be composed of {110} and {100} facets, [35,36] graphene/Au(110) and graphene/Au(100) were employed as models of the Au@rGO structure (Fig. S10A and S10B). The charge distribution is visualized in the electrostatic potential mapping images (Fig. 4A and 4B), in which red Indicates negative and blue positive

potential. In both graphene/Au(110) and graphene/Au(100) systems, the color in the vicinity of the top surface Au atoms change to deeper blue when combined with graphene, suggesting the electron-deficiency of the top surface Au atoms. The average Mulliken charges of Au and C atoms were summarized in Table S1. In both graphene/Au models, the top surface Au atoms are positively charged compared with the monometallic Au model, and the C atoms are negatively charged than the graphene, which indicates that electrons in the Au surface are transferred to the graphene layer at the Au/graphene interface. Therefore, it is assumed that SPR-induced hot-electrons generated at the surface of Au NRs are likely to move to the rGO layer in Pd/Au@rGO-10/SiO_2 catalyst, leading the longer-time electron-hole separation. This is also supported by the reported experimental observation that SPR-induced electrons can be transferred from Au NPs to contiguous graphene. [37-39]

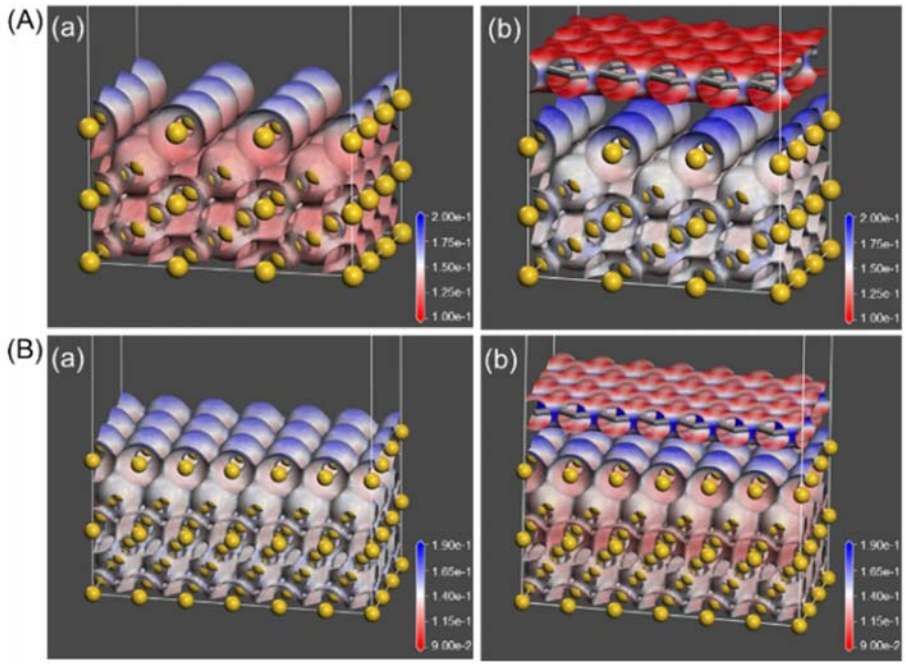

Figure 4. Electrostatic potential mappings over electron density iso-surface of (A) (a) (3×3) Au(110) surface cell and (b) (5×2) graphene surpercell on (3×3) Au(110) surface cell, and (B) (a)

(6×3) Au(100) surface cell and (b) (7×2) graphene surpercell on (6×3) Au(100) surface cell. The iso-surfaces are drawn at 0.2 e/Å^3.

Based on the above-mentioned characterization and reaction results, the catalyst structure and a plausible reaction-promotion mechanism of Pd/Au@rGO-10/SiO_2 are illustrated in Figure 5. When visible-light is irradiated on the catalyst, light can pass through the rGO layer, and reach the surfaces of Au NRs. The SPR of Au NRs is excited and electron-hole pairs are generated mainly at the ends of the long axis, the so-called tips, of the NRs because of the anisotropic structure. [20,40] The electronically conductive rGO layer can act as an electron mediator and transfer the hot-electrons from the tips of Au NRs to the Pd active sites quickly. On the Pd clusters, hot-electrons would be injected into the lowest unoccupied molecular orbital (LUMO) of the adsorbed iodobenzene and lead to weakening of the C−I bond, which accelerates the coupling reaction.[16,17,41,42] In the previous reports of catalysts in which Pd species are directly deposited on the Au NR surface, it was believed that hot-electrons generated in the tips of Au NRs cannot be efficiently transferred to the Pd species on the cylinder-sides of Au NRs because of the ultrafast decay of SPR-induced hot-electrons, resulted in a low reaction promotion even under visible-light irradiation.[40,43] This is consistent with the low (1.5-fold) activity enhancement of Pd/Au/SiO_2 without an rGO layer. Previously reported Pd-Au or Pd-Ag type plasmonic catalysts also show only around 1.5 times activity enhancement in the Suzuki-Miyaura coupling reaction under visible-light irradiation.[42,44] On the other hand, the rGO layer in Pd/Au@rGO-10/SiO_2 would promote the longer-time electron-hole separation and efficiently carry hot-electrons from Au NRs to Pd active sites. Thus, Pd/Au@rGO-10/SiO_2 exhibits 4-fold activity enhancement under visible-light irradiation. Moreover, it has been reported that SPR-induced hot-electrons quickly decay at the

Pd/Au interfaces, and therefore the plasmonic nanostructures having smaller Pd-Au interface area show the longer lifetime of hot-electrons, resulted in the higher catalytic activity.[20] The lifetime of hot-electrons would be prolonged in the Pd/Au@rGO structure compared to Pd/Au, because the rGO layer spatially separates Pd from Au and minimizes the Pd/Au interfaces, which also leads to the large activity enhancement of the Pd/Au@rGO-10/SiO_2 catalyst.

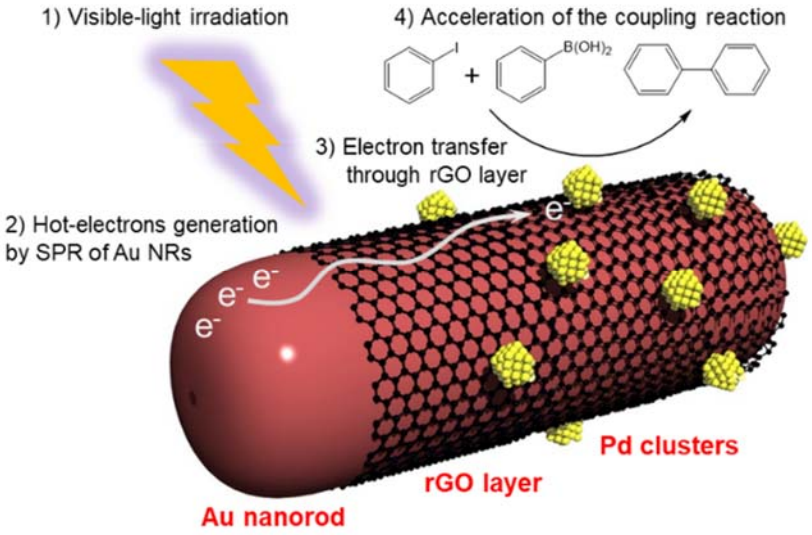

Figure 5. Reaction promotion mechanism under visible-light irradiation of Pd/Au@rGO-10/SiO_2.

Conclusions

In summary, we developed Pd clusters supported on an rGO-coated Au NRs catalyst and demonstrated that the SPR-induced large activity enhancement can be obtained under visible-light irradiation in the Suzuki-Miyaura coupling reaction. In such a structure-controlled catalytic system, hot-electrons, generated by the SPR of Au NRs under visible-light, are efficiently carried to the

Pd active sites *via* the rGO layer, and thus the catalytic reaction is promoted. Our study presents a novel approach to maximizing the utilization efficiency of SPR-induced hot-electrons, providing a design guideline for developing highly active plasmonic catalysts

ASSOCIATED CONTENT

Supporting Information. TG and DTA profiles, EDX spectra, Raman spectra, wavelength-dependent catalytic activity of the prepared catalysts, TEM images and UV-vis spectra of the reference catalysts, and DFT calculation results.

AUTHOR INFORMATION

Corresponding Author

*E-mail: yamashita@mat.eng.osaka-u.ac.jp. Tel./Fax: +81-(0)6-6879-7457.

ORCID

Yasutaka Kuwahara: 0000-0002-5867-6463

Kohsuke Mori: 0000-0003-3915-4528

Hiromi Yamashita: 0000-0003-1796-5776

Notes

The authors declare no competing financial interest.

ACKNOWLEDGMENT

The present work was supported by a Grant-in-Aid for Scientific Research (KAKENHI No. 26220911) from the Japan Society for the Promotion of Science (JSPS). T.Y. thanks JSPS for a

Research Fellowship for Young Scientists (No. 18J20246). Y. K., K. M., and H. Y. thank MEXT program ‘‘Elements Strategy Initiative for Catalysts & Batteries (ESICB)’’.

REFERENCES

(1) Liz-Marzán, L. M.; Murphy, C. J.; Wang, J. Nanoplasmonics. *Chem. Soc. Rev.* **2014**, *43*, 3820–3822.

(2) Brongersma, M. L.; Halas, N. J.; Nordlander, P. Plasmon-Induced Hot Carrier Science and Technology. *Nat. Nanotechnol.* **2015**, *10*, 25–34.

(3) Marimuthu, A.; Zhang, J.; Linic, S. Tuning Selectivity in Propylene Epoxidation by Plasmon Mediated Photo-Switching of Cu Oxidation State. *Science,* **2013**, *339*, 1590–1593.

(4) Linic, S.; Christopher, P.; Ingram, D. B. Plasmonic-Metal Nanostructures for Efficient Conversion of Solar to Chemical Energy. *Nat. Mater.* **2011**, *10*, 911–921.

(5) Fuku, K.; Hayashi, R.; Takakura, S.; Kamegawa, T.; Mori, K.; Yamashita, H. The Synthesis of Size- and Color-Controlled Silver Nanoparticles by Using Microwave Heating and Their Enhanced Catalytic Activity by Localized Surface Plasmon Resonance. *Angew. Chem. Int. Ed.* **2013**, *52*, 7446–7450.

(6) Mori, K.; Kawashima, M.; Che, M.; Yamashita, H. Enhancement of the Photoinduced Oxidation Activity of a Ruthenium(II) Complex Anchored on Silica-Coated Silver Nanoparticles by Localized Surface Plasmon Resonance. *Angew. Chem. Int. Ed.* **2010**, *49*, 8598–8601.

(7) Kuwahara, Y.; Yoshimura, Y.; Haematsu, K.; Yamashita, H. Mild Deoxygenation of Sulfoxides over Plasmonic Molybdenum Oxide Hybrid with Dramatic Activity Enhancement under Visible Light. *J. Am. Chem. Soc.* **2018**, *140*, 9203-9210.

(8) Christopher, P.; Xin, H.; Linic, S. Visible-Light-Enhanced Catalytic Oxidation Reactions on Plasmonic Silver Nanostructures. *Nat. Chem.* **2011**, *3*, 467–472.

(9) Boerigter, C.; Campana, R.; Morabito, M.; Linic, S. Evidence and Implications of Direct Charge Excitation as the Dominant Mechanism in Plasmon-Mediated Photocatalysis. *Nat. Commun.* **2016**, *7*, 10545.

(10) Zhang, X.; Li, X.; Zhang, D.; Su, N. Q.; Yang, W.; Everitt, H. O.; Liu, J. Product Selectivity in Plasmonic Photocatalysis for Carbon Dioxide Hydrogenation. *Nat. Commun.* **2017**, *8*, 14542.

(11) Kale, M. J.; Avanesian, T.; Xin, H.; Yan, J.; Christopher, P. Controlling Catalytic Selectivity on Metal Nanoparticles by Direct Photoexcitation of Adsorbate-Metal Bonds. *Nano Lett.* **2014**, *14*, 5405–5412.

(12) Yang, J.; Li, Y.; Zu, L.; Tong, L.; Liu, G.; Qin, Y.; Shi, D. Light-Concentrating Plasmonic Au Superstructures with Significantly Visible-Light-Enhanced Catalytic Performance. *ACS Appl. Mater. Interfaces* **2015**, *7*, 8200–8208.

(13) Song, H.; Meng, X.; Dao, T. D.; Zhou, W.; Liu, H.; Shi, L.; Zhang, H.; Nagao, T.; Kako, T.; Ye, J. Light-Enhanced Carbon Dioxide Activation and Conversion by Effective Plasmonic Coupling Effect of Pt and Au Nanoparticles. *ACS Appl. Mater. Interfaces* **2018**, *10*, 408–416.

(14) Ingram, D. B.; Linic, S. Photoelectrodes : Evidence for Selective Plasmon-Induced Formation. *J. Am. Chem. Soc.* **2011**, *133*, 5202–5205.

(15) Ueno, K.; Misawa, H. Plasmon-Enhanced Photocurrent Generation and Water Oxidation from Visible to near-Infrared Wavelengths. *NPG Asia Mater.* **2013**, *5*, e61.

(16) Wang, F.; Li, C.; Chen, H.; Jiang, R.; Sun, L.-D.; Li, Q.; Wang, J.; Yu, J. C.; Yan, C.-H. Plasmonic Harvesting of Light Energy for Suzuki Coupling Reactions. *J. Am. Chem. Soc.* **2013**, *135*, 5588–5601.

(17) Kang, E.; Shin, H.; Lim, D.-K. Interface-Controlled Pd Nanodot-Au Nanoparticle Colloids for Efficient Visible-Light-Induced Photocatalytic Suzuki-Miyaura Coupling Reaction. *Catalysts* **2018**, *8*, 463.

(18) Lin, S. C.; Hsu, C. S.; Chiu, S. Y.; Liao, T. Y.; Chen, H. M. Edgeless Ag-Pt Bimetallic Nanocages: In Situ Monitor Plasmon-Induced Suppression of Hydrogen Peroxide Formation. *J. Am. Chem. Soc.* **2017**, *139*, 2224–2233.

(19) Chen, H.; Wang, F.; Li, K.; Woo, K. C.; Wang, J.; Li, Q.; Sun, L. D.; Zhang, X.; Lin, H. Q.; Yan, C. H. Plasmonic Percolation: Plasmon-Manifested Dielectric-to-Metal Transition. *ACS Nano* **2012**, *6*, 7162–7171.

(20) Guo, J.; Zhang, Y.; Shi, L.; Zhu, Y.; Mideksa, M. F.; Hou, K.; Zhao, W.; Wang, D.; Zhao, M.; Zhang, X.; et al. Boosting Hot Electrons in Hetero-Superstructures for Plasmon-Enhanced Catalysis. *J. Am. Chem. Soc.* **2017**, *139*, 17964–17972.

(21) Geim, A. K.; Novoselov, K. S. The Rise of Graphene. *Nat. Mater.* **2007**, *6*, 183–191.

(22) Hummers, W. S.; Offeman, R. E. Preparation of Graphitic Oxide. *J. Am. Chem. Soc.* **1958**, *80*, 1339.

(22) Lim, D.-K.; Barhoumi, A.; Wylie, R. G.; Reznor, G.; Langer, R. S.; Kohane, D. S. Enhanced Photothermal Effect of Plasmonic Nanoparticles Coated with Reduced Graphene Oxide. *Nano Lett.* **2013**, *13*, 4075–4079.

(24) Gole, A.; Murphy, C. J. Seed-Mediated Synthesis of Gold Nanorods: Role of the Size and Nature of the Seed. *Chem. Mater.* **2004**, *16*, 3633–3640.

(25) Ming, T.; Zhao, L.; Yang, Z.; Chen, H.; Sun, L.; Wang, J.; Yan, C. Strong Polarization Dependence of Plasmon-Enhanced of Plasmon-Enhanced FluoresStrong Polarization Dependenccence on Single Gold Nanorods. *Nano Lett.* **2009**, *9*, 3896–3903.

(26) Delley, B. An All-Electron Numerical Method for Solving the Local Density Functional for Polyatomic Molecules. *J. Chem. Phys.* **1990**, *92*, 508–517.

(27) Delley, B. From Molecules to Solids with the DMol^3 Approach. *J. Chem. Phys.* **2000**, *113*, 7756–7764.

(28) Yang, S.; Feng, X.; Ivanovici, S.; Müllen, K. Fabrication of Graphene-Encapsulated Oxide Nanoparticles: Towards High-Performance Anode Materials for Lithium Storage. *Angew. Chem. Int. Ed.* **2010**, *49*, 8408–8411.

(29) Çiplak, Z.; Yildiz, N.; Çalimli, A. Investigation of Graphene/Ag Nanocomposites Synthesis Parameters for Two Different Synthesis Methods. *Fullerenes, Nanotub. Carbon Nanostructures* **2015**, *23*, 361–370.

(30) Shin, H.-J.; Kim, K. K.; Benayad, A.; Yoon, S.-M.; Park, H. K.; Jung, I.-S.; Jin, M. H.; Jeong, H.-K.; Kim, J. M.; Choi, J.-Y. et al. Efficient Reduction of Graphite Oxide by Sodium Borohydride and Its Effect on Electrical Conductance. *Adv. Funct. Mater.* **2009**, *19*, 1987-1992.

(31) Liu, S. Y.; Huang, L.; Li, J. F.; Wang, C.; Li, Q.; Xu, H. X.; Guo, H. L.; Meng, Z. M.; Shi, Z.; Li, Z. Y. Simultaneous Excitation and Emission Enhancement of Fluorescence Assisted by Double Plasmon Modes of Gold Nanorods. *J. Phys. Chem. C* **2013**, *117*, 10636–10642.

(32) Liu, H.; Zhang, G.; Zhou, Y.; Gao, M.; Yang, F. One-Step Potentiodynamic Synthesis of Poly(1,5-Diaminoanthraquinone)/ Reduced Graphene Oxide Nanohybrid with Improved Electrocatalytic Activity. *J. Mater. Chem. A* **2013**, *1*, 13902–13913.

(33) Xue, C.; Zhang, T.; Ding, S.; Wei, J.; Yang, G. Anchoring Tailored Low-Index Faceted BiOBr Nanoplates onto TiO2Nanorods to Enhance the Stability and Visible-Light-Driven Catalytic Activity. *ACS Appl. Mater. Interfaces* **2017**, *9*, 16091–16102.

(34) Zhang, S.; Chang, C.; Huang, Z.; Ma, Y.; Gao, W.; Li, J.; Qu, Y. Visible-Light-Activated Suzuki–Miyaura Coupling Reactions of Aryl Chlorides over the Multifunctional Pd/Au/Porous Nanorods of CeO_2 Catalysts. *ACS Catal.* **2015**, 5, 6481–6488.

(35) Wang, Z. L.; Mohamed, M. B.; Link, S.; El-Sayed, M. A. Crystallographic Facets and Shapes of Gold Nanorods of Different Aspect Ratios. *Surf. Sci.* **1999**, *440*, 809–814.

(36) Goris, B.; Bals, S.; Van den Broek, W.; Carbó-Argibay, E.; Gómez-Graña, S.; Liz-Marzán, L. M.; Van Tendeloo, G. Atomic-Scale Determination of Surface Facets in Gold Nanorods. *Nat. Mater.* **2012**, *11*, 930–935.

(37) Xia, Z.; Li, P.; Wang, Y.; Song, T.; Zhang, Q.; Sun, B. Solution-Processed Gold Nanorods Integrated with Graphene for Near-Infrared Photodetection via Hot Carrier Injection. *ACS Appl. Mater. Interfaces* **2015**, *7*, 24136–24241.

(38) Hoggard, A.; Wang, L. Y.; Ma, L.; Fang, Y.; You, G.; Olson, J.; Liu, Z.; Chang, W. S.; Ajayan, P. M.; Link, S. Using the Plasmon Linewidth to Calculate the Time and Efficiency of Electron Transfer between Gold Nanorods and Graphene. *ACS Nano* **2013**, *7*, 11209–11217.

(39) Kumar, D.; Lee, A.; Lee, T.; Lim, M.; Lim, D. K. Ultrafast and Efficient Transport of Hot Plasmonic Electrons by Graphene for Pt Free, Highly Efficient Visible-Light Responsive Photocatalyst. *Nano Lett.* **2016**, *16*, 1760–1767.

(40) Zheng, Z.; Tachikawa, T.; Majima, T. Plasmon-Enhanced Formic Acid Dehydrogenation Using Anisotropic Pd–Au Nanorods Studied at the Single-Particle Level. *J. Am. Chem. Soc.* **2015**, *137*, 948–957.

(41) Xiao, Q.; Sarina, S.; Bo, A.; Jia, J.; Liu, H.; Arnold, D. P.; Huang, Y.; Wu, H.; Zhu, H. Visible Light-Driven Cross-Coupling Reactions at Lower Temperatures Using a Photocatalyst of Palladium and Gold Alloy Nanoparticles. *ACS Catal.* **2014**, *4*, 1725–1734.

(42) Verma, P.; Kuwahara, Y.; Mori, K.; Yamashita, H. Pd/Ag and Pd/Au Bimetallic Nanocatalysts on Mesoporous Silica for Plasmon-Mediated Enhanced Catalytic Activity under Visible Light Irradiation. *J. Mater. Chem. A* **2016**, *4*, 10142–10150.

(43) Yin, Y.; Yang, Y.; Zhang, L.; Li, Y.; Li, Z.; Lei, W.; Ma, Y.; Huang, Z. Facile Synthesis of Au/Pd Nano-Dogbones and Their Plasmon-Enhanced Visible-to-NIR Light Photocatalytic Performance. *RSC Adv.* **2017**, *7*, 36923–36928.

(44) Wen, M.; Takakura, S.; Fuku, K.; Mori, K.; Yamashita, H. Enhancement of Pd-Catalyzed Suzuki-Miyaura Coupling Reaction Assisted by Localized Surface Plasmon Resonance of Au Nanorods. *Catal. Today* **2015**, *242*, 381–385.

TOC Graphic

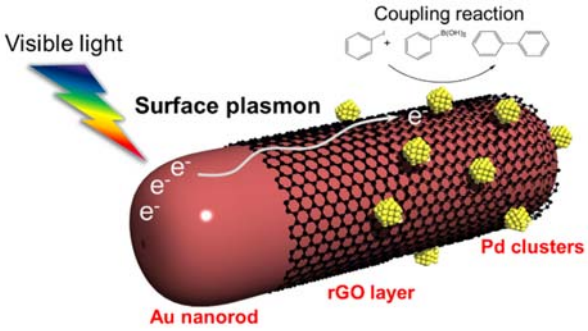
Coupling reaction
Visible light
Surface plasmon
e-
e-
e-
e-
Pd clusters
rGO layer
Au nanorod